CMS Physics Analysis Summary

Contact: cms-pag-conveners-heavyions@cern.ch 2023/06/21

Observation of enhanced long-range elliptic anisotropies inside high-multiplicity jets in pp collisions at the LHC

The CMS Collaboration

Abstract

A search for QCD collective effects is performed with the CMS experiment via correlation measurements of charged constituents inside jets produced in proton-proton collisions at the LHC. The analysis uses data collected at a center-of-mass energy of $\sqrt{s}$ = 13 TeV, corresponding to an integrated luminosity of 138 fb^{-1}. For charged constituents within a reconstructed jet of cone radius 0.8, two-particle correlations as functions of relative azimuthal angle ($\Delta\phi^*$) and pseudorapidity ($\Delta\eta^*$) are performed in a novel "jet frame," where constituent η, ϕ variables are redefined relative to the direction of the jet. The correlation functions are studied in classes of in-jet charged-particle multiplicity up to nearly 100. Anisotropy Fourier harmonics are extracted from long-range azimuthal correlation functions for $|\Delta\eta^*| > 2$. For low-multiplicity jets, the long-range elliptic anisotropy harmonic, v_2^{j}, is observed to decrease with multiplicity. This trend is well described by Monte Carlo (MC) event generators. However, a rising trend of v_2^{j} emerges at an in-jet charged-particle multiplicity above ≈ 80. This trend is not reproduced by MC models. This observation yields new insights into the dynamics of parton fragmentation processes in the vacuum.

This document has been revised with respect to the version dated June 21, 2023.

Quantum chromodynamics (QCD) describes the behavior and properties of particles that couple to the strong force. The nonperturbative nature of QCD at low energies leads to the phenomenon of color confinement, where quarks and gluons, collectively known as partons, are sequestered inside of hadrons. A consequence of color confinement is that no color-charged partons exist in isolation, and only color-neutral particles can be found in nature. 'Hard scattering' events between color-neutral particles such as protons can result in collimated sprays of hadrons originating from the fragmentation and hadronization of an energetic parton. This collimated spray is called a "jet." The dynamics of parton fragmentation that lead to jet structures are not yet fully understood from first principles of QCD because they involve nonperturbative, many-body processes. Experimentally accessible jets are typically highly energetic and can occasionally generate large final-state hadron multiplicities (e.g., more than 100 charged particles) resulting from an initial parton.

Final states containing thousands of hadrons are routinely produced in high-energy nuclear collisions, where a hot, dense medium of nearly free partons known as a quark-gluon plasma (QGP) is formed. The extreme parton densities realized in these collisions result in strong partonic rescatterings, which quickly drive the system evolution toward the nearly ideal hydrodynamic limit. As a result, striking long-range collective flow effects have been observed and extensively studied using the azimuthal correlations of particles emitted over a wide pseudorapidity (η) range (also known as the "ridge") at the Relativistic Heavy Ion Collider [1–4] and the CERN LHC [5–9].

It was thought that small collision systems such as electron-positron (e^+e^-), electron-proton (ep), and proton-proton (pp) collisions were too small and dilute for there to be a sufficient number of secondary partonic rescatterings to drive the system toward thermal equilibrium. For this reason, collective hydrodynamic behavior was not expected in these systems. Surprisingly, similar long-range collective azimuthal correlations have been discovered in pp collisions with large final-state particle multiplicity [10–13], which raised the question of whether a tiny QGP droplet is created [14]. Subsequently, such collective phenomena have been observed in additional small systems, such as proton-nucleus (pA) collisions [15–24], and lighter nucleus-nucleus (AA) systems [24–27]. Searches for QCD collective effects were also recently extended to e^+e^- [28, 29], ep [30, 31], photon-proton (γp) [32] and photonuclear (γA) [33] systems but limited to relatively low-multiplicity events (less than 30-40 charged particles).

The natural compelling question to address is: from how small of a partonic system – and under what conditions – can collectivity emerge? In Ref. [34], it is postulated that QCD collective effects can be initiated by systems as small as a scattered parton as it traverses through the vacuum and hadronizes into a high-multiplicity final state. This is illustrated in Fig. 1. Motivated by that idea, this note presents a search for such collective effects inside of individual jets (as opposed to full events) produced in pp collisions at $\sqrt{s} = 13$ TeV using the CMS experiment at the LHC. This search examines the possibility that a sufficiently large number of rescatterings among partonic "showers," during the fragmentation of a very high multiplicity jet, could lead to the flow-like behavior seen in QGP. Using a coordinate system defined with respect to the jet axis, which is a proxy for the direction of the parton initiating the jet, the two-particle correlation function of charged constituents of a jet is measured as a function of the charged-particle multiplicity, $N^{\mathrm{j}}_{\mathrm{ch}}$, inside the jet. The anisotropy Fourier coefficients ($V^{\mathrm{j}}_{n\Delta}$) of long-range (i.e., large η separation) azimuthal correlations are then extracted and compared to Monte Carlo (MC) event generators modeling the parton fragmentation process.

The CMS apparatus [35] is a multipurpose, nearly hermetic detector, designed to trigger on [36, 37] and identify electrons, muons, photons, and (charged and neutral) hadrons [38–40]. A

global "particle-flow" (PF) algorithm [41] aims to reconstruct all individual particles in an event, combining information provided by the all-silicon inner tracker and by the crystal electromagnetic and brass-scintillator hadron calorimeters, operating inside a 3.8 T superconducting solenoid, with data from the gas-ionization muon detectors embedded in the flux-return yoke outside the solenoid. The reconstructed particles are used to build τ leptons, jets, and missing transverse momentum [42–44].

The $\sqrt{s} = 13\,\text{TeV}$ pp collisions used in this analysis were collected from 2016 to 2018 and correspond to an integrated luminosity of 138 fb^{-1}. The data were collected using an online trigger searching for events containing anti-k_T jets [45, 46] with radius parameter R = 0.8 having a transverse momentum (p_T) above 500 GeV. In the offline analysis, jets were required to have a $p_\text{T} > 550\,\text{GeV}$ to maintain a trigger efficiency above 50%. To correct for the remaining trigger inefficiency, each jet receives a weight corresponding to the inverse of the trigger efficiency at that jet's p_T. To ensure the jet constituents fall within the acceptance of the CMS tracker (i.e., $|\eta| < 2.4$), jets are also required to have $|\eta| < 1.6$ in the laboratory reference frame.

The two primary MC generators used in this analysis are PYTHIA8 [47] with the CP5 tune [48] and SHERPA [49] . The leading order PYTHIA8 uses the Lund String fragmentation model which is based on long range nonperturbative QCD from lattice computations and treats color fields as QCD flux tubes, the breaking of which leads to new $\text{q}\overline{\text{q}}$ pairs. SHERPA uses a cluster model which is based on next-to-leading order pQCD calculations and groups quarks and gluons into color neutral clusters from which hadronization occurs. These MC generators also differ in their parton shower models and therefore provide materially different baseline comparisons to data. The PYTHIA8 events are input into Geant4 to emulate the response of the CMS detector for the purposes of calculating correction factors.

Jet momentum is determined as the vectorial sum of all particle momenta in the jet and is found from MC simulation to be, on average, within 5 to 10% of the true momentum over the whole p_T spectrum and detector acceptance. Additional pp interactions within the same or nearby bunch crossings ("pileup") can contribute additional tracks and calorimetric energy depositions, increasing the apparent jet momentum. The pileup per particle identification algorithm (PUPPI) [50, 51] is used to mitigate the effect of pileup at the reconstructed particle level, making use of local shape information, event pileup properties, and tracking information.

This analysis is particularly interested in the charged particle constituents of jets. These charged particles are explicitly required to have $|\eta| < 2.4$ and $p_\text{T} > 0.3\,\text{GeV}$ in the laboratory reference frame. Additional selections requiring a relative p_T uncertainty of less than 10%, and a distance of closest approach significance with respect to the primary vertex of at least three standard deviations (σ), are applied to ensure high-quality tracks are used. Jets are then classified into different classes based on the number of charged particles passing these selections (N^j_ch).

Jet energy corrections are derived from MC simulation studies so that the average measured energy of jets becomes identical to that of particle-level jets. In situ measurements of the momentum balance in dijet, γ + jet, Z + jet, and QCD multijet events are used to determine any residual differences between the jet energy scale in data and in MC simulation, and appropriate corrections are made [43]. Additional selection criteria are applied to each jet to remove jets potentially dominated by instrumental effects or reconstruction failures. The jet energy resolution is typically 10% at 100 GeV, and 5% at 1 TeV [43].

The two-particle correlation analysis is similar to that employed in Ref. [15], except that the momentum vectors of all charged-particle constituents of a jet are defined in the "jet frame". Figure 1 illustrates this new coordinate system, along with the idea that a fragmenting parton

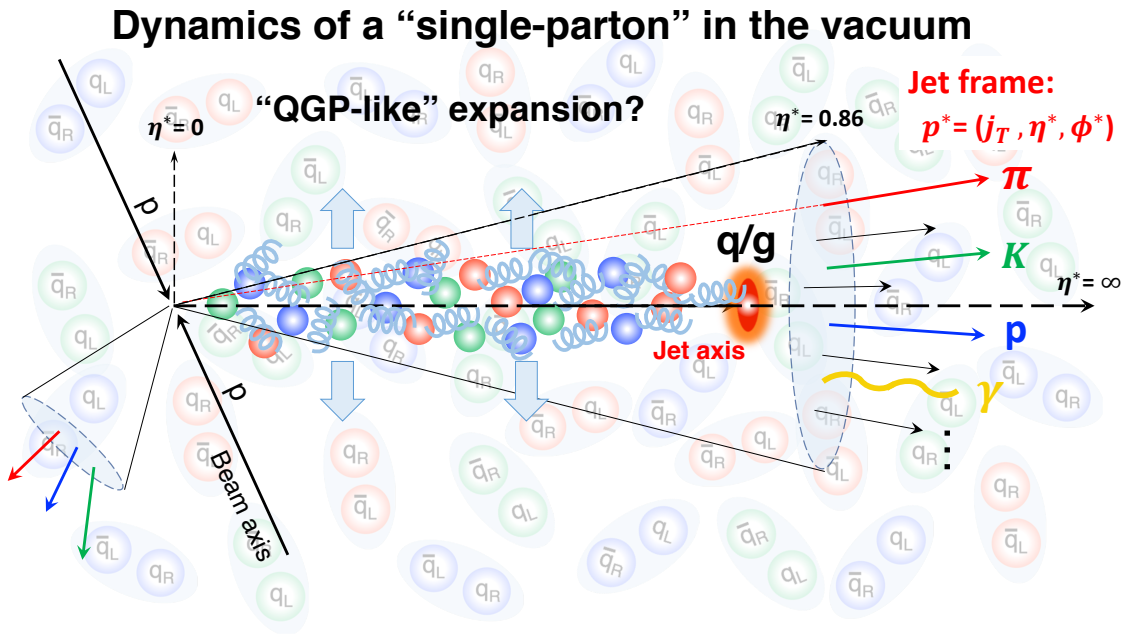

Figure 1: A schematic illustration of a jet and its constituents in a pp collision, showing the idea of an initial scattered parton eventually exhibiting potential collective expansion in the direction transverse to the jet axis. A jet cone and emerging final state particles are drawn in a coordinate system, denoted the “jet frame”, where the z axis coincides with the jet direction. Cone size is not to scale.

could exhibit collectivity, as discussed in [34]. A unique jet reference frame is defined for every jet such that the z-axis is aligned with the direction of jet momentum. Momentum vectors of charged particle constituents are redefined in this new frame, are redefined in this new frame, $\vec{p}^* = (j_T, \eta^*, \phi^*)$. Here, j_T is the particle transverse momentum with respect to the jet axis. The symbols η^* and ϕ^* are the pseudorapidity and azimuthal angle coordinates with respect to the jet axis, respectively. Therefore, $\eta^* = 0$ and ∞ correspond to vectors that are perpendicular and parallel to the jet axis, as illustrated in Fig. 1. In this system, $\eta^* = 0.86$ is the approximate boundary of an anti-k_{T} jet with a cone size 0.8. The azimuthal coordinate of tracks approximately parallel to the direction of the jet axis ($\eta^* > 5$) is sensitive to small changes in the jet axis direction caused by resolution effects. Thus, these tracks are excluded in the subsequent analysis procedure. Reconstructed particles in the event that are not clustered into the jet of interest are not considered in the analysis. For each jet with $p_{\mathrm{T}} > 550\,\mathrm{GeV}$, the two-dimensional (2D) angular correlation function is calculated using jet's charged-particle constituents as follows:

$$\frac{1}{N_{\mathrm{ch}}^{\mathrm{trg}}} \frac{\mathrm{d}^2 N^{\mathrm{pair}}}{\mathrm{d}\Delta\eta^* \mathrm{d}\Delta\phi^*} = B(0,0) \frac{S(\Delta\eta^*, \Delta\phi^*)}{B(\Delta\eta^*, \Delta\phi^*)}, \tag{1}$$

where $\Delta\eta^*$ and $\Delta\phi^*$ are the relative pseudorapidity and azimuthal angle in the jet frame for a pair of trigger and associate particles in a given j_{T} range. If more than one jet is found in an event, they are treated independently. The measurement is performed as a function of $N_{\mathrm{ch}}^{\mathrm{j}}$ and repeated for three different j_{T} ranges. The functions $S(\Delta\eta^*, \Delta\phi^*)$ and $B(\Delta\eta^*, \Delta\phi^*)$ represent the

signal and background distributions, respectively:

$$S(\Delta\eta^*, \Delta\phi^*) = \frac{1}{N_{\mathrm{ch}}^{\mathrm{trg}}} \frac{\mathrm{d}^2 N^{\mathrm{sig}}}{\mathrm{d}\Delta\eta^* \mathrm{d}\Delta\phi^*}, \tag{2}$$

and

$$B(\Delta\eta^*, \Delta\phi^*) = \frac{1}{N_{\mathrm{ch}}^{\mathrm{trg}}} \frac{\mathrm{d}^2 N^{\mathrm{bkg}}}{\mathrm{d}\Delta\eta^* \mathrm{d}\Delta\phi^*}. \tag{3}$$

The $S(\Delta\eta^*, \Delta\phi^*)$ distribution is calculated with pairs taken from charged-particle constituents of each jet and then averaged over all jets, weighted by the jet $N_{\mathrm{ch}}^{\mathrm{j}}$. The background distribution serves as both a reference and a correction to the pair acceptance due to the limited η^* range. To construct the $B(\Delta\eta^*, \Delta\phi^*)$ distribution, a 2D single-particle η^*–ϕ^* distribution for charged-particle constituents of all jets is first derived. Pairs of points from this distribution are then randomly selected to construct $B(\Delta\eta^*, \Delta\phi^*)$. In this way, correlations in the background distribution are related to single-particle distributions and/or detector effects, and the $B(0,0)/B(\Delta\eta^*, \Delta\phi^*)$ term in Eq. 1 is the appropriate pair acceptance correction to the signal distribution. During this procedure a correction for tracking inefficiency is applied by weighting each charged particle constituent by the inverse of the track reconstruction efficiency, which is calculated using samples of simulated events.

The resulting 2D distribution can be further studied by decomposition into a one-dimensional (1D) Fourier series:

$$\frac{1}{N_{\mathrm{ch}}^{\mathrm{trg}}} \frac{\mathrm{d}N^{\mathrm{pair}}}{\mathrm{d}\Delta\phi^*} \propto 1 + 2 \sum_{n=1}^{\infty} V_{\mathrm{n}\Delta} \cos(\mathrm{n}\Delta\phi^*), \tag{4}$$

By taking 1D $\Delta\phi^*$ projections over $|\Delta\eta^*| > 2$, short-range correlations are excluded, highlighting the azimuthal correlation structures for large-η^* separations. The strength of the Fourier components in this decomposition could give indications of the existence of collective effects and their relative significance in various systems. Of particular interest is the second Fourier component, which is typically associated with the strength of elliptic anisotropies. The single-particle elliptic anisotropy Fourier coefficient, v_2^{j}, is the main observation of interest and is related to the two-particle Fourier coefficient as $v_2^{\mathrm{j}} = \sqrt{V_{2\Delta}^{\mathrm{j}}}$. Results are presented as a function of the average $N_{\mathrm{ch}}^{\mathrm{j}}$ inside a jet after correcting for detector effects, $\left\langle N_{\mathrm{ch}}^{\mathrm{j}} \right\rangle$.

The primary sources of systematic uncertainty come from the jet axis pointing resolution, the jet p_{T} resolution, residual pileup effects (after applying the PUPPI algorithm), and the tracking efficiency. These four sources are added together in quadrature to calculate the total systematic uncertainty. To reduces the effects of statistical fluctuations, the four highest multiplicity classes examined in this analysis are treated together when evaluating the magnitudes of systematic effects. The effect of the jet pointing resolution is examined by smearing each jet axis in the 2D $\eta - \phi$ plane according to the resolution calculated in simulated MC samples. The coordinate transformation of constituents' momenta, η^*, and ϕ^* into the jet reference frame is recalculated with the new smeared jet axis, and the analysis procedure is repeated. The difference of $V_{n\Delta}^{\mathrm{j}}$ values before and after this smearing process is taken as the systematic uncertainty resulting from the jet pointing resolution. The impact of this effect on $V_{n\Delta}^{\mathrm{j}}$ is between 0.01 and 0.04 (depending on the j_{T} range examined) at lower charged particle multiplicities, where jet constituents tend to have a narrower angular distribution and therefore larger changes to their jet frame kinematic values for a given jet axis variation. On the other hand, this uncertainty is

<0.001 at higher charged particle multiplicities because these jets tend to have a wider angular separation from the jet axis on average. The effects of the *uncertainty* in the overall scale of the jet p_{T} correction are negligible for this analysis. However, a similar smearing procedure found the uncertainty in $V^{\mathrm{j}}_{n\Delta}$ coming from the jet p_{T} *resolution* to range from 0 to 0.002. The systematic uncertainty coming from residual pileup effects is estimated by splitting the data set into two roughly equal subsets. The root mean square of the deviations of each of these two subsets from the nominal result is taken as the uncertainty in $V^{\mathrm{j}}_{n\Delta}$ from this source. For $V^{\mathrm{j}}_{2\Delta}$, this uncertainty ranges from 0.001 to 0.003. Additional cross checks using smaller data subsets containing even higher and lower pileup values, as well as subsets separated by data collection year, were found to give consistent results. An additional study was performed to evaluate the sensitivity of this analysis to pileup using the particle weights provided by the PUPPI algorithm, which can be interpreted as a probability that the particle originates from a signal vertex as opposed to a pileup vertex [51]. The nominal result includes all charged particles having nonzero PUPPI weight. A more stringent selection requiring a PUPPI weight above 0.85 was found to have no substantial impact on the final results. The systematic uncertainty resulting from the tracking efficiency correction is evaluated by applying more and less stringent track selections, repeating the analysis procedure, and calculating the root means square of the deviations of these variations from the nominal case. The uncertainty in $V^{\mathrm{j}}_{2\Delta}$ from this source reaches a maximum value of 0.003.

Figure 2 shows an example of 2D two-particle angular correlation functions in the jet frame for inclusive and high-$N^{\mathrm{j}}_{\mathrm{ch}}$ jets for charged particles in the range $0.3 < j_{\mathrm{T}} < 3\,\mathrm{GeV}$. The $\left\langle N^{\mathrm{j}}_{\mathrm{ch}} \right\rangle$ is 26 and 101 for the two classes of jets shown. The high-$N^{\mathrm{j}}_{\mathrm{ch}}$ jet class corresponds to a fraction of only 2×10^{-5} of all jets with $p_{\mathrm{T}} > 550\,\mathrm{GeV}$. The central peak at $(\Delta\eta^*, \Delta\phi^*) = (0, 0)$, truncated for better visualization, is the result of short-range correlations from the parton shower and hadronization. The far-side ridge at $\Delta\eta^* \approx \pi$ is mostly related to back-to-back particle production and conservation of momentum. These prominent features have also been found in lab-frame analyses of pp collisions [10], where they can also be reproduced using MC simulations. This indicates that the dynamics of bulk hadron production in the parton fragmentation process may share similarities to those of a hadron-hadron collision process. Moreover, a feature commonly observed in AA collisions is the near-side enhancement at $\Delta\phi^* \approx 0$ over long-range in $\Delta\eta^*$, commonly known as the near-side "ridge". The $N^{\mathrm{j}}_{\mathrm{ch}}$ reached in the single jet system of this work is comparable to the event multiplicity of pp collisions where a near-side ridge was first observed using a laboratory frame analysis [10]. There appears to be some indication of a near-side ridge in the high-$N^{\mathrm{j}}_{\mathrm{ch}}$ plot in Fig 2 out to $\Delta\eta^* = 3$, however this feature is less prominent than the ridges observed in pp and pA collisions. There is no corresponding near-side enhancement observed in the 2D distributions in either PYTHIA8 or SHERPA .

To examine features of the long-range azimuthal correlations in detail, 1D $\Delta\phi^*$ correlation functions averaged over $|\Delta\eta^*| > 2$ are displayed in Fig. 3, for particles with $0.3 < j_{\mathrm{T}} < 3\,\mathrm{GeV}$ in two $N^{\mathrm{j}}_{\mathrm{ch}}$ classes. Results from PYTHIA8 and SHERPA simulations over the corresponding $N^{\mathrm{j}}_{\mathrm{ch}}$ ranges are also shown for comparison. For high- and inclusive $N^{\mathrm{j}}_{\mathrm{ch}}$ classes in data, PYTHIA8 and SHERPA, we find strong away-side correlations consistent with dominant contributions of back-to-back momentum conservation effects. For inclusive $N^{\mathrm{j}}_{\mathrm{ch}}$ jets in the data (top left), the near-side at $\Delta\phi^* \sim 0$ clearly shows a minimum. However, for highest-$N^{\mathrm{j}}_{\mathrm{ch}}$ jets studied in data, with $\left\langle N^{\mathrm{j}}_{\mathrm{ch}} \right\rangle$=101, (bottom left) an indication of a near-side enhancement is seen, which is not present in PYTHIA8 or SHERPA events having comparable $N^{\mathrm{j}}_{\mathrm{ch}}$ (bottom right). The Fourier fits

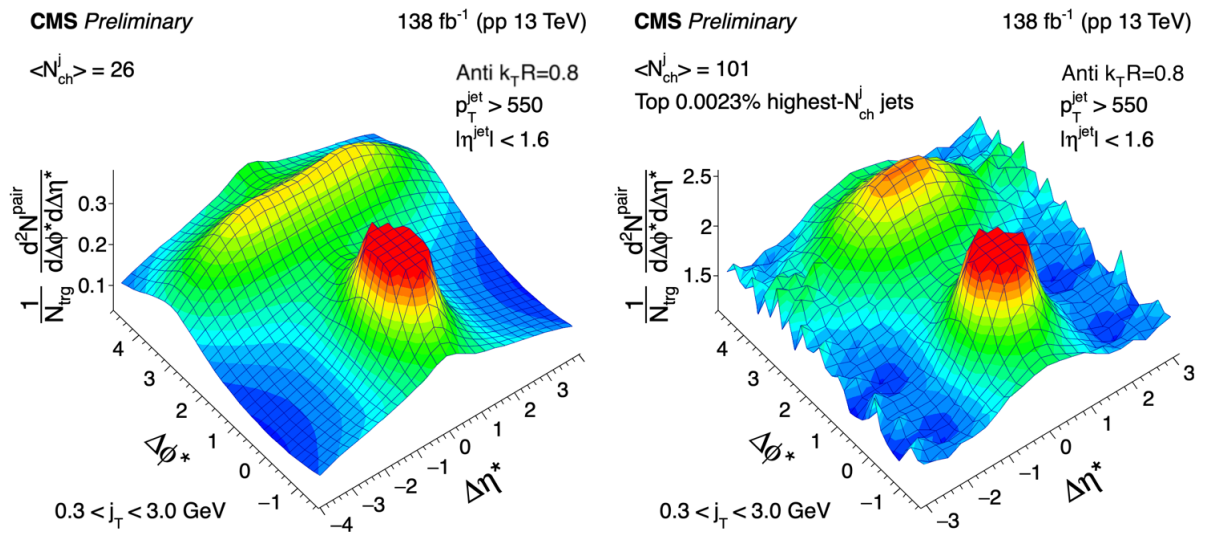

Figure 2: Examples of 2D two-particle angular correlation functions for particle $0.3 < j_T < 3$ GeV from all jet multiplicities (left) and the highest (right) in-jet N^j_{ch}, for anti-k_T R = 0.8 jets with jet $p_T > 550$ GeV and $|\eta| < 1.6$.

of the correlation functions used to extract $V^j_{n\Delta}$ are also shown and are dominated by a negative $V_{1\Delta}$ component. The addition of more Fourier terms has little impact on the first three Fourier coefficients.

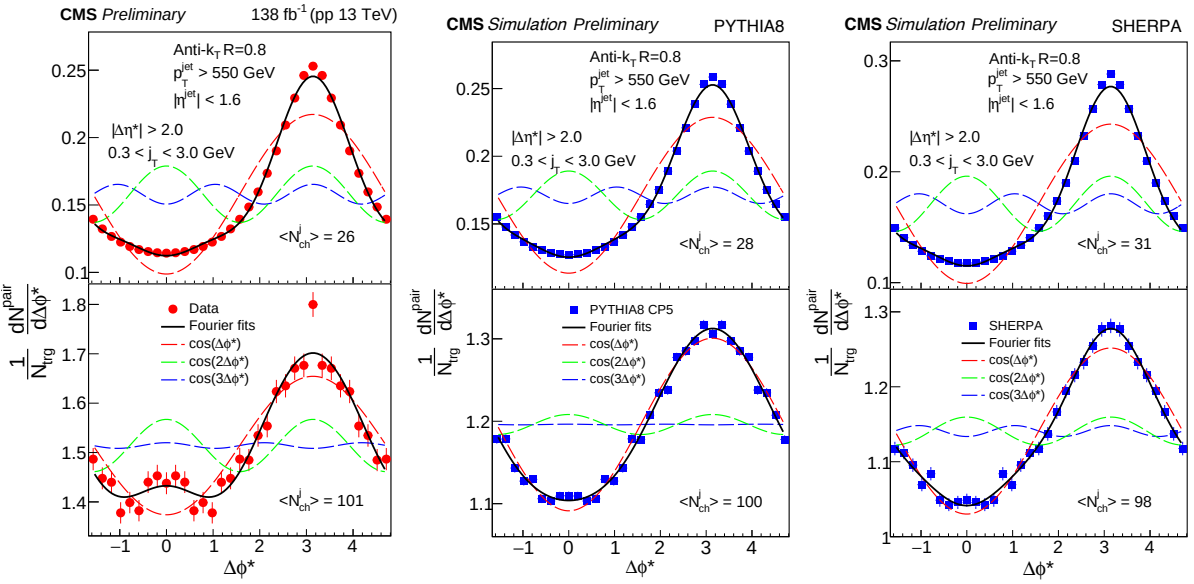

Figure 3: Examples of 1D two-particle angular correlation functions projected on $\Delta\phi^*$ for particles in the range $0.3 < j_T < 3$ GeV and $|\Delta\eta^*| > 2$, for two in-jet N^j_{ch} classes in data (left) , PYTHIA8 (middle), and SHERPA (right). The solid black line shows the fitted Fourier function and the colored dashed lines show the individual Fourier components. Vertical bars on data points indicate statistical uncertainty

The extracted two-particle Fourier coefficients for the first three harmonics $V^j_{n\Delta}$, as a function of the in-jet (N^j_{ch}), are shown in Figure 4 (left). Over the full N^j_{ch} range, the odd-order harmonics, $V^j_{1\Delta}$ and $V^j_{3\Delta}$, are negative, while $V^j_{2\Delta}$ is positive. The magnitudes of all harmonics tend

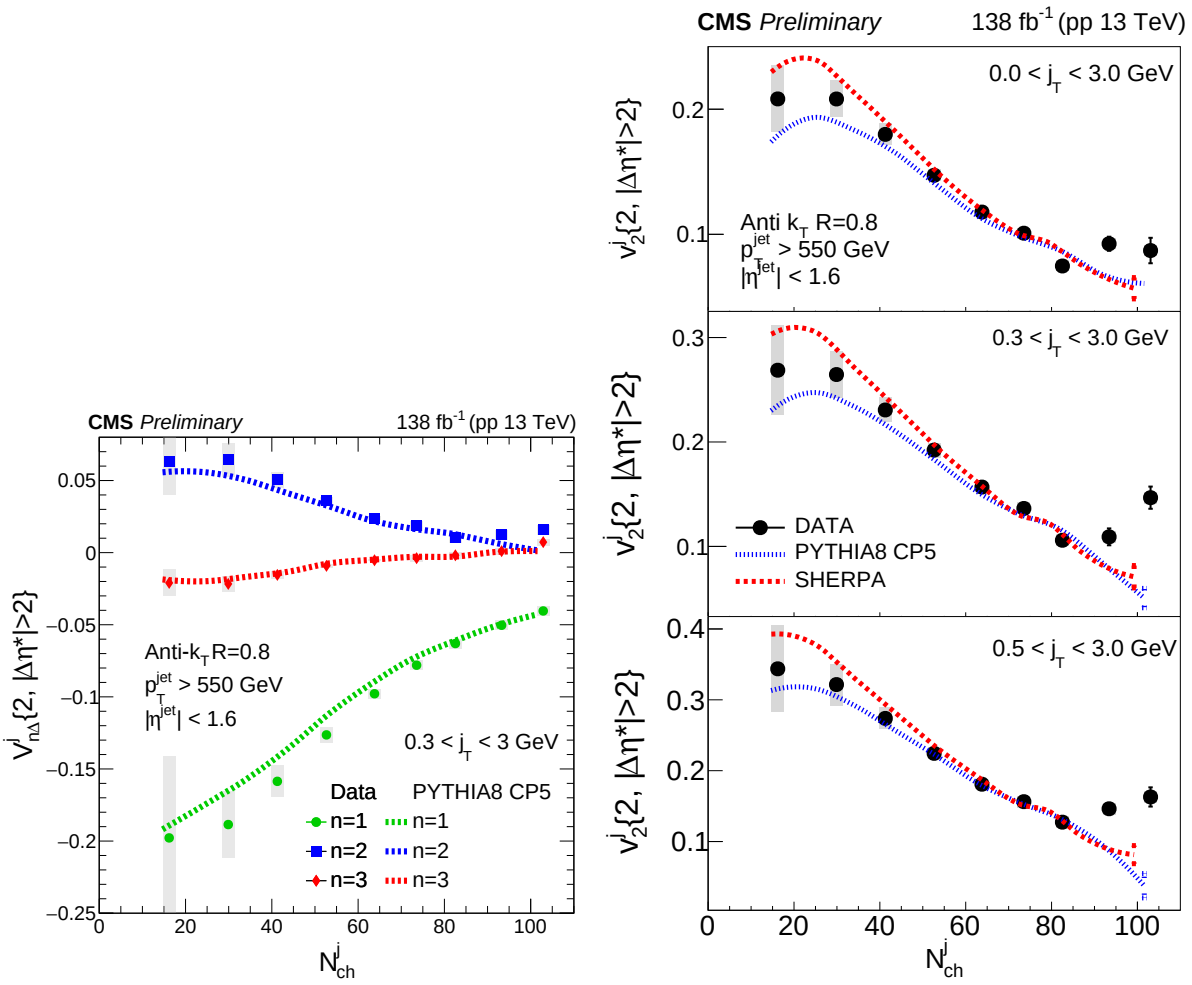

Figure 4: The extracted two-particle Fourier coefficients $V^{j}_{n\Delta}$ (left) and single-particle elliptic anisotropies $v^{j}_{2}\{2\}$ (right), as a function of N^{j}_{ch}, for anti-k_T R=0.8 jets with jet $p_T > 550$ GeV and $|\eta| < 1.6$ jets in pp collisions at 13 TeV from data, PYTHIA8, and SHERPA . Vertical bars on data points indicate statistical uncertainty in the extracted Fourier component. Vertical grey bands indicate the total systematic uncertainty.

to decrease as N^{j}_{ch} increases. All these features are consistent with expectation of short-range back-to-back correlations, as observed in lab-frame analyses, that are not related to collective effects. This is because the contribution of short-range few-body correlations to the two-particle Fourier coefficient is expected to diminish at a rate proportional to $\approx 1/N^{j}_{ch}$. The PYTHIA8 generator is generally successful in describing the experimental data for all three Fourier harmonics over a wide N^{j}_{ch} range. There appears to be a slight deviation in $V^{j}_{2\Delta}$ between data and simulation, as well as a $V^{j}_{3\Delta}$ which turns positive in data at the highest N^{j}_{ch}.

Figure 4 (right) shows the single-particle elliptic anisotropies $v^{j}_{2}\{2\}$, in the jet frame, as a function of N^{j}_{ch} inside the jet (N^{j}_{ch}). Here, results for three different j_T ranges are shown for data, PYTHIA8 and SHERPA events. Again, the MC simulation is generally successful at describing the data over a wide N^{j}_{ch} range in all three j_T ranges. For jets at $N^{j}_{ch} > 80$, however, the value $v^{j}_{2}\{2\}$ no longer diminishes as $1/N^{j}_{ch}$, as would be expected if only short-range few-body correlation are present. Instead, the data start to show a steady increases with N^{j}_{ch}. Such an

increase of $v_2^j\{2\}$ for very high-N_{ch}^j jets is not observed in either PYTHIA8 or SHERPA and may be an indication of the onset of new QCD effects, e.g., collectivity, in the parton fragmentation processes.

The increasing trend of $v_2^j\{2\}$ with N_{ch}^j in the data is observed for all three j_T ranges investigated. To quantify this rise, a linear fit to the three highest multiplicity bins was performed using both data and simulated samples. For the j_T ranges of $0.3-3.0\,\text{GeV}$ and $0.5-3.0\,\text{GeV}$, the difference of the slopes extracted from data and both PYTHIA8 and SHERPA has a significance greater than 5σ. The non-monotonic dependence of $v_2^j\{2\}$ versus N_{ch}^j is not expected if few-body processes are the dominant sources of the observed correlations, and may indicate novel QCD phenomena related to nonperturbative dynamics of a parton fragmenting in the vacuum. These phenomena could include the emergence of collective effects driven by secondary partonic rescatterings, as suggested in Ref. [34]. Further experimental and theoretical inputs are still needed to investigate the physical origin of the observed enhancement.

In summary, the first search for long-range near-side correlations and QCD collective effects in jets produced in 13 TeV pp collisions is presented. The measurement is performed using a jet's charged particle constituents, after their kinematic variables have been calculated in a reference frame where the z-axis is defined as the jet direction. Two-particle correlations are studied as a function of the number of charged particle constituents in the jet, N_{ch}^j, which extends to values of over 100, and the transverse momentum with respect to the jet direction.

The first three Fourier harmonics of long-range azimuthal correlations are extracted and compared with those of the PYTHIA8 and SHERPA Monte Carlo (MC) event generators. While data and the MC samples are in good agreement for particle correlations inside low- and mid-N_{ch}^j jets, the extracted long-range elliptic azimuthal anisotropy $v_2^j\{2\}$ shows a distinct increase in data for $N_{ch}^j > 80$. Such a feature is not observed in any of MC event generators that model the parton fragmentation process. Therefore, results presented in this note may pave a new direction in uncovering novel effects related to nonperturbative QCD dynamics of parton fragmentation in the vacuum.

References

[1] STAR Collaboration, "Distributions of charged hadrons associated with high transverse momentum particles in pp and AuAu collisions at $\sqrt{s_{NN}} = 200\,\text{GeV}$", *Phys. Rev. Lett.* **95** (2005) 152301, doi:10.1103/PhysRevLett.95.152301, arXiv:nucl-ex/0501016.

[2] PHOBOS Collaboration, "System size dependence of cluster properties from two-particle angular correlations in CuCu and AuAu collisions at $\sqrt{s_{NN}} = 200\,\text{GeV}$", *Phys. Rev. C* **81** (2010) 024904, doi:10.1103/PhysRevC.81.024904, arXiv:0812.1172.

[3] STAR Collaboration, "Long range rapidity correlations and jet production in high energy nuclear collisions", *Phys. Rev. C* **80** (2009) 064912, doi:10.1103/PhysRevC.80.064912, arXiv:0909.0191.

[4] PHOBOS Collaboration, "High transverse momentum triggered correlations over a large pseudorapidity acceptance in AuAu collisions at $\sqrt{s_{NN}} = 200\,\text{GeV}$", *Phys. Rev. Lett.* **104** (2010) 062301, doi:10.1103/PhysRevLett.104.062301, arXiv:0903.2811.

[5] CMS Collaboration, "Long-range and short-range dihadron angular correlations in central PbPb collisions at a nucleon-nucleon center of mass energy of 2.76 TeV", *JHEP* **07** (2011) 076, doi:10.1007/JHEP07(2011)076, arXiv:1105.2438.

[6] CMS Collaboration, "Centrality dependence of dihadron correlations and azimuthal anisotropy harmonics in PbPb collisions at $\sqrt{s_{\mathrm{NN}}} = 2.76$ TeV", *Eur. Phys. J. C* **72** (2012) 2012, doi:10.1140/epjc/s10052-012-2012-3, arXiv:1201.3158.

[7] ALICE Collaboration, "Elliptic flow of charged particles in PbPb collisions at 2.76 TeV", *Phys. Rev. Lett.* **105** (2010) 252302, doi:10.1103/PhysRevLett.105.252302, arXiv:1011.3914.

[8] ATLAS Collaboration, "Measurement of the azimuthal anisotropy for charged particle production in $\sqrt{s_{\mathrm{NN}}} = 2.76$ TeV lead-lead collisions with the ATLAS detector", *Phys. Rev. C* **86** (2012) 014907, doi:10.1103/PhysRevC.86.014907, arXiv:1203.3087.

[9] CMS Collaboration, "Studies of azimuthal dihadron correlations in ultra-central PbPb collisions at $\sqrt{s_{\mathrm{NN}}} = 2.76$ TeV", *JHEP* **02** (2014) 088, doi:10.1007/JHEP02(2014)088, arXiv:1312.1845.

[10] CMS Collaboration, "Observation of long-range near-side angular correlations in proton-proton collisions at the LHC", *JHEP* **09** (2010) 091, doi:10.1007/JHEP09(2010)091, arXiv:1009.4122.

[11] ATLAS Collaboration, "Observation of long-range elliptic azimuthal anisotropies in $\sqrt{s_{\mathrm{NN}}} = 13$ and 2.76 TeV pp collisions with the ATLAS detector", *Phys. Rev. Lett.* **116** (2016) 172301, doi:10.1103/PhysRevLett.116.172301, arXiv:1509.04776.

[12] CMS Collaboration, "Measurement of long-range near-side two-particle angular correlations in pp collisions at $\sqrt{s_{\mathrm{NN}}} = 13$ TeV", *Phys. Rev. Lett.* **116** (2016) 172302, doi:10.1103/PhysRevLett.116.172302, arXiv:1510.03068.

[13] CMS Collaboration, "Evidence for collectivity in pp collisions at the LHC", *Phys. Lett. B* **765** (2017) 193, doi:10.1016/j.physletb.2016.12.009, arXiv:1606.06198.

[14] K. Dusling, W. Li, and B. Schenke, "Novel collective phenomena in high-energy proton-proton and proton-nucleus collisions", *Int. J. Mod. Phys. E* **25** (2016) 1630002, doi:10.1142/S0218301316300022, arXiv:1509.07939.

[15] CMS Collaboration, "Observation of long-range near-side angular correlations in proton-lead collisions at the LHC", *Phys. Lett. B* **718** (2013) 795, doi:10.1016/j.physletb.2012.11.025, arXiv:1210.5482.

[16] ALICE Collaboration, "Long-range angular correlations on the near and away side in pPb collisions at $\sqrt{s_{\mathrm{NN}}} = 5.02$ TeV", *Phys. Lett. B* **719** (2013) 29, doi:10.1016/j.physletb.2013.01.012, arXiv:1212.2001.

[17] ATLAS Collaboration, "Observation of associated near-side and away-side long-range correlations in $\sqrt{s_{\mathrm{NN}}} = 5.02$ TeV proton-lead collisions with the ATLAS detector", *Phys. Rev. Lett.* **110** (2013), no. 18, 182302, doi:10.1103/PhysRevLett.110.182302, arXiv:1212.5198.

[18] LHCb Collaboration, "Measurements of long-range near-side angular correlations in $\sqrt{s_{\mathrm{NN}}} = 5$ TeV proton-lead collisions in the forward region", *Phys. Lett. B* **762** (2016) 473, doi:10.1016/j.physletb.2016.09.064, arXiv:1512.00439.

[19] ALICE Collaboration, "Long-range angular correlations of pi, K and p in p–Pb collisions at $\sqrt{s_{\rm NN}} = 5.02$ TeV", *Phys. Lett. B* **726** (2013) 164, doi:10.1016/j.physletb.2013.08.024, arXiv:1307.3237.

[20] CMS Collaboration, "Long-range two-particle correlations of strange hadrons with charged particles in pPb and PbPb collisions at LHC energies", *Phys. Lett. B* **742** (2015) 200, doi:10.1016/j.physletb.2015.01.034, arXiv:1409.3392.

[21] CMS Collaboration, "Evidence for collective multi-particle correlations in pPb collisions", *Phys. Rev. Lett.* **115** (2015) 012301, doi:10.1103/PhysRevLett.115.012301, arXiv:1502.05382.

[22] ATLAS Collaboration, "Measurement of multi-particle azimuthal correlations in pp, pPb and low-multiplicity PbPb collisions with the ATLAS detector", *Eur. Phys. J. C* **77** (2017) 428, doi:10.1140/epjc/s10052-017-4988-1, arXiv:1705.04176.

[23] ATLAS Collaboration, "Measurement of long-range multiparticle azimuthal correlations with the subevent cumulant method in pp and pPb collisions with the ATLAS detector at the CERN Large Hadron Collider", *Phys. Rev. C* **97** (2018) 024904, doi:10.1103/PhysRevC.97.024904, arXiv:1708.03559.

[24] PHENIX Collaboration, "Creation of quark-gluon plasma droplets with three distinct geometries", *Nature Phys.* **15** (2019) 214, doi:10.1038/s41567-018-0360-0, arXiv:1805.02973.

[25] STAR Collaboration, "Long-range pseudorapidity dihadron correlations in dAu collisions at $\sqrt{s_{\rm NN}} = 200$ GeV", *Phys. Lett. B* **747** (2015) 265, doi:10.1016/j.physletb.2015.05.075, arXiv:1502.07652.

[26] PHENIX Collaboration, "Measurements of elliptic and triangular flow in high-multiplicity ^{3}HeAu collisions at $\sqrt{s_{\rm NN}} = 200$ GeV", *Phys. Rev. Lett.* **115** (2015) 142301, doi:10.1103/PhysRevLett.115.142301, arXiv:1507.06273.

[27] PHENIX Collaboration, "Measurements of Multiparticle Correlations in dAu Collisions at 200, 62.4, 39, and 19.6 GeV and pAu Collisions at 200 GeV and Implications for Collective Behavior", *Phys. Rev. Lett.* **120** (2018) 062302, doi:10.1103/PhysRevLett.120.062302, arXiv:1707.06108.

[28] A. Badea et al., "Measurements of two-particle correlations in e^+e^- collisions at 91 GeV with ALEPH archived data", *Phys. Rev. Lett.* **123** (2019) 212002, doi:10.1103/PhysRevLett.123.212002, arXiv:1906.00489.

[29] Belle Collaboration, "Measurement of Two-Particle Correlations of Hadrons in e^+e^- Collisions at Belle", *Phys. Rev. Lett.* **128** (2022) 142005, doi:10.1103/PhysRevLett.128.142005, arXiv:2201.01694.

[30] ZEUS Collaboration, "Two-particle azimuthal correlations as a probe of collective behaviour in deep inelastic ep scattering at HERA", *JHEP* **04** (2020) 070, doi:10.1007/JHEP04(2020)070, arXiv:1912.07431.

[31] ZEUS Collaboration, "Azimuthal correlations in photoproduction and deep inelastic ep scattering at HERA", *JHEP* **12** (2021) 102, doi:10.1007/JHEP12(2021)102, arXiv:2106.12377.

[32] CMS Collaboration, "Two-particle azimuthal correlations in γp interactions using pPb collisions at $\sqrt{s_{\mathrm{NN}}}$ = 8.16 TeV", 4, 2022. arXiv:2204.13486.

[33] ATLAS Collaboration, "Two-particle azimuthal correlations in photonuclear ultraperipheral PbPb collisions at 5.02 TeV with ATLAS", *Phys. Rev. C* **104** (2021) 014903, doi:10.1103/PhysRevC.104.014903, arXiv:2101.10771.

[34] A. Baty, P. Gardner, and W. Li, "Collective evolution of a parton in the vacuum: the ultimate partonic "droplet", non-perturbative QCD and quantum entanglement", 4, 2021. arXiv:2104.11735.

[35] CMS Collaboration, "The CMS experiment at the CERN LHC", *JINST* **3** (2008) S08004, doi:10.1088/1748-0221/3/08/S08004.

[36] CMS Collaboration, "Performance of the CMS Level-1 trigger in proton-proton collisions at $\sqrt{s_{\mathrm{NN}}} = 13$ TeV", *JINST* **15** (2020) P10017, doi:10.1088/1748-0221/15/10/P10017, arXiv:2006.10165.

[37] CMS Collaboration, "The CMS trigger system", *JINST* **12** (2017) P01020, doi:10.1088/1748-0221/12/01/P01020, arXiv:1609.02366.

[38] CMS Collaboration, "Electron and photon reconstruction and identification with the CMS experiment at the CERN LHC", *JINST* **16** (2021) P05014, doi:10.1088/1748-0221/16/05/P05014, arXiv:2012.06888.

[39] CMS Collaboration, "Performance of the CMS muon detector and muon reconstruction with proton-proton collisions at $\sqrt{s_{\mathrm{NN}}} = 13$ TeV", *JINST* **13** (2018) P06015, doi:10.1088/1748-0221/13/06/P06015, arXiv:1804.04528.

[40] CMS Collaboration, "Description and performance of track and primary-vertex reconstruction with the CMS tracker", *JINST* **9** (2014) P10009, doi:10.1088/1748-0221/9/10/P10009, arXiv:1405.6569.

[41] CMS Collaboration, "Particle-flow reconstruction and global event description with the CMS detector", *JINST* **12** (2017) P10003, doi:10.1088/1748-0221/12/10/P10003, arXiv:1706.04965.

[42] CMS Collaboration, "Performance of reconstruction and identification of τ leptons decaying to hadrons and ν_τ in pp collisions at $\sqrt{s_{\mathrm{NN}}} = 13$ TeV", *JINST* **13** (2018) P10005, doi:10.1088/1748-0221/13/10/P10005, arXiv:1809.02816.

[43] CMS Collaboration, "Jet energy scale and resolution in the CMS experiment in pp collisions at 8 TeV", *JINST* **12** (2017) P02014, doi:10.1088/1748-0221/12/02/P02014, arXiv:1607.03663.

[44] CMS Collaboration, "Performance of missing transverse momentum reconstruction in proton-proton collisions at $\sqrt{s_{\mathrm{NN}}} = 13$ TeV using the CMS detector", *JINST* **14** (2019) P07004, doi:10.1088/1748-0221/14/07/P07004, arXiv:1903.06078.

[45] M. Cacciari, G. P. Salam, and G. Soyez, "The anti-k_t jet clustering algorithm", *JHEP* **04** (2008) 063, doi:10.1088/1126-6708/2008/04/063, arXiv:0802.1189.

[46] M. Cacciari, G. P. Salam, and G. Soyez, "FastJet user manual", *Eur. Phys. J. C* **72** (2012) 1896, doi:10.1140/epjc/s10052-012-1896-2, arXiv:1111.6097.

[47] T. Sjostrand, S. Mrenna, and P. Z. Skands, "A brief introduction to PYTHIA 8.1", *Comput. Phys. Commun.* **178** (2008) 852, doi:10.1016/j.cpc.2008.01.036, arXiv:0710.3820.

[48] CMS Collaboration, "Extraction and validation of a new set of CMS PYTHIA8 tunes from underlying-event measurements", *Eur. Phys. J. C* **80** (2020), no. 1, 4, doi:10.1140/epjc/s10052-019-7499-4, arXiv:1903.12179.

[49] Sherpa Collaboration, "Event generation with Sherpa 2.2", *SciPost Phys.* **7** (2019), no. 3, 034, doi:10.21468/SciPostPhys.7.3.034, arXiv:1905.09127.

[50] CMS Collaboration, "Pileup mitigation at CMS in 13 TeV data", *JINST* **15** (2020) P09018, doi:10.1088/1748-0221/15/09/p09018, arXiv:2003.00503.

[51] D. Bertolini, P. Harris, M. Low, and N. Tran, "Pileup per particle identification", *JHEP* **10** (2014) 059, doi:10.1007/JHEP10(2014)059, arXiv:1407.6013.